

## Reciprocal Oscillons and Nonmonotonic Fronts in Forced Nonequilibrium Systems

Arik Yochelis,\* John Burke, and Edgar Knobloch

Department of Physics, University of California, Berkeley, California 94720, USA  
(Received 27 April 2006; published 22 December 2006)

The formation of oscillons in a synchronously oscillating background is studied in the context of both damped and self-exciting oscillatory media. Using the forced complex Ginzburg-Landau equation we show that such states bifurcate from finite amplitude homogenous states near the 2:1 resonance boundary. In each case we identify a region in parameter space containing a finite multiplicity of coexisting stable oscillons with different structure. Stable time-periodic monotonic and nonmonotonic frontlike states are present in an overlapping region. Both types of structure are related to the presence of a Maxwell point between the zero and finite amplitude homogeneous states.

DOI: 10.1103/PhysRevLett.97.254501

PACS numbers: 47.20.Ky, 46.40.Ff, 47.54.-r

Time-dependent spatially localized structures called oscillons [1,2] can be observed in a wide range of driven dissipative systems [2–4]. States of this type usually form through a subharmonic instability of a periodically driven system; i.e., the resulting oscillons oscillate at close to half the forcing frequency  $\Omega$ . Two types of oscillons can be distinguished. The best understood are those that are embedded in a nonoscillating spatially homogeneous background [5]. More recently, however, localized oscillations have been found in which the homogeneous background also oscillates with frequency near  $\Omega/2$ . In such systems the localized structure therefore oscillates synchronously with the background [3], and may be thought of as a “hole” in an oscillating background. In this Letter we refer to these states as *reciprocal* oscillons, and identify their origin and properties.

Experiments on granular media subjected to vertical vibration [6] and on the oscillatory Belousov-Zhabotinsky (BZ) chemical reaction [7] reveal that reciprocal oscillons are present in a narrow parameter range near the onset of labyrinthine patterns, which in turn form as finite amplitude patterns near the boundary of the 2:1 resonance tongue [6,8]. These results suggest that the observable reciprocal oscillons also develop in the vicinity of the resonance boundary. In this Letter we show, through a bifurcation analysis of a model equation, that a large multiplicity of coexisting stable but distinct reciprocal oscillons is present in a specific region of parameter space, and show that the presence of these states is intimately related to the existence of multiple stable frontlike states with both monotonic and nonmonotonic profiles. This phenomenon is related to the presence of a Maxwell point between two spatially homogeneous states; such Maxwell points are present in both self-exciting and damped driven systems.

We begin with an oscillatory system with natural frequency close to  $\Omega/2$  near a supercritical bifurcation to spatially uniform oscillations. In such systems a dynamical observable  $w$  takes the form

$$w = w_0 + Ae^{i\Omega t/2} + \text{c.c.} + \dots, \quad (1)$$

where  $w_0$  represents the equilibrium state,  $A$  is a complex amplitude, and the ellipses denote higher order terms. The oscillation amplitude  $A$  obeys the forced complex Ginzburg-Landau (FCGL) equation [9]

$$A_t = (\mu + i\nu)A - (1 + i\beta)|A|^2A + (1 + i\alpha)\nabla^2A + \gamma A^*, \quad (2)$$

where  $\mu$  represents the distance from the onset of the instability,  $\nu$  is the detuning from the unforced frequency, and  $\alpha$ ,  $\beta$ , and  $\gamma$  represent dispersion, nonlinear frequency correction, and the amplitude of the forcing, respectively. Here  $A^*$  is the complex conjugate of  $A$  and  $\nabla^2$  is the two-dimensional Laplacian operator. In the absence of forcing ( $\gamma = 0$ ) the system oscillates spontaneously when  $\mu > 0$ ; for  $\mu < 0$  uniform oscillations are damped.

The uniform stationary solutions of Eq. (2) correspond to homogeneous subharmonic oscillations phase-locked to the forcing, and take the form  $A_{n\pi} \equiv R_{\pm} \exp(i\phi_{n\pi})$  where  $R_{\pm} \equiv \sqrt{\tilde{\mu} \pm \tilde{\gamma}/\varrho}$  is real, and  $\phi_{n\pi} \equiv 2^{-1} \arcsin[(\nu - \beta R_{\pm}^2)/\gamma] + n\pi$ . Here  $\tilde{\mu} \equiv \mu + \nu\beta$ ,  $\tilde{\gamma} \equiv \sqrt{\varrho^2\gamma^2 - \tilde{\nu}^2}$ ,  $\tilde{\nu} \equiv \nu - \mu\beta$ , and  $\varrho \equiv \sqrt{1 + \beta^2}$ . The integer  $n$  indicates a state that is in phase with the forcing ( $n = 0$ ) or out of phase ( $n = 1$ ); both have identical stability properties. When  $\tilde{\mu} > 0$  the phase-locked states  $R = R_-$  appear via a subcritical bifurcation from  $R = 0$  at  $\gamma = \gamma_0 \equiv \sqrt{\mu^2 + \nu^2}$  and are unstable. These annihilate with stable  $R = R_+$  states at a saddle-node bifurcation at  $\gamma = \gamma_b \equiv |\nu - \mu\beta|/\varrho$ . Thus the region  $\gamma_b < \gamma < \gamma_0$  corresponds to coexistence between the two spatially homogeneous states  $R = 0$  and  $R = R_+$  [9,10]. Figure 1 shows this region for both  $\mu < 0$  and  $\mu > 0$ , together with sample spatially localized states (insets) obtained by integrating Eq. (2) in two dimensions for parameter values in this region.

The key to the presence of localized states is held by Eq. (2) in one spatial dimension. The equation, linearized about  $A = A_{n\pi}$ , has solutions of the form

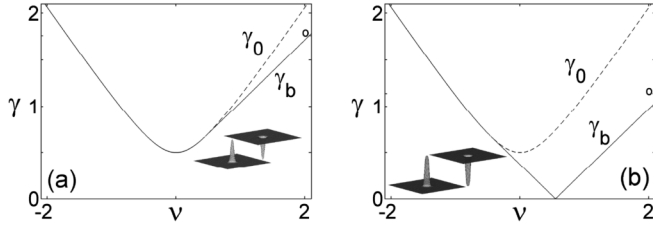


FIG. 1. Boundaries of the 2:1 resonance tongue for the FCGL Eq. (2) in the  $(\nu, \gamma)$  plane for (a)  $\mu = -0.5$  (damped case), and (b)  $\mu = 0.5$  (self-exciting case). Open circles indicate the location of stable two-dimensional reciprocal oscillons obtained via direct numerical integration on  $x = [0, 80]$ ,  $y = [0, 80]$  with Neumann boundary conditions, and shown in the form of  $\text{Re}A(x, y)$  in the insets at two times separated by the forcing period  $2\pi/\Omega$ . (a)  $\gamma = 1.76$ , (b)  $\gamma = 1.14$ , with  $\nu = 2.0$ ,  $\alpha = 1$ ,  $\beta = 1.1$  in both cases.

$A - A_{n\pi} \propto \exp(\lambda x)$ , where the spatial eigenvalue  $\lambda$  satisfies a fourth order algebraic equation. At  $\gamma = \gamma_b$  the homogeneous phase-locked states  $A_{n\pi}$  have two zero spatial eigenvalues; when  $\mu(1 - \beta^2 + 2\alpha\beta) + \nu[2\beta - \alpha(1 - \beta^2)] > 0$  (the case considered here) one of the remaining eigenvalues is positive and the other negative. In this case weakly nonlinear analysis near  $\gamma = \gamma_b$  reveals the presence of small amplitude reciprocal oscillons of the form [11]

$$A_r(x) = A_{n\pi} + 3b(\xi + i)\text{sech}^2(\sqrt{a/2}x) \cos(n\pi). \quad (3)$$

These states can be followed numerically [12] away from  $\gamma = \gamma_b$ . Figure 2 shows the result when  $\mu < 0$ ,  $0 < \alpha < \beta$  in terms of the norm

$$\|A\| = \sqrt{\frac{1}{L} \int_{-L/2}^{L/2} \{|A|^2 + |\partial_x A|^2\} dx}, \quad (4)$$

where  $L$  is the spatial domain size. The state  $|A| = R_+$  is also indicated. Inspection shows that (3) agrees well with the hole profiles computed numerically near the saddle-node line  $\gamma = \gamma_b$  [Fig. 2(a)].

Stability calculations show that the small amplitude reciprocal oscillons that emerge from  $\gamma = \gamma_b$  are unstable but gain stability at a saddle node [see point (b) in Fig. 2]. The reciprocal oscillons branch then oscillates with decreasing amplitude about  $\gamma = \gamma_M$ , forming an alternating sequence of stable and unstable states (see Fig. 2). We refer to the point  $\gamma = \gamma_M$  as a Maxwell point by analogy with the corresponding point familiar from variational systems [13]. At this unique point the  $A_r$  states turn into a pair of stationary fronts connecting  $A = 0$  to  $A_{n\pi}$  and  $A_{n\pi}$  back to  $A = 0$ . Since the states  $A = 0$ ,  $A_{n\pi}$  are spatially uniform, no broadening of the Maxwell point due to pinning effects takes place [13]; consequently the  $A_r$  branch ultimately collapses to the Maxwell point (see Fig. 2) as the holes deepen enough to interact with the  $A = 0$  state [see Fig. 2(d)].

In addition, we find a second family of large-amplitude states to which we refer as nonmonotonic fronts. To follow the latter we initialized our continuation scheme using one half ( $-L/2 < x < 0$ ) of the  $A_r$  solution at  $\gamma_M$  [see (d) in Fig. 2] and imposed odd symmetry at  $x = 0$ . In contrast to the reciprocal oscillons  $A_r$ , the frontlike states  $A_f$  come in from large  $\gamma$  [Fig. 2(h)] as stable monotonic (Ising) fronts [10]. Thus we identify the reciprocal oscillons with homoclinic connections of a phase-locked state  $A_{n\pi}$  to itself, while the nonmonotonic fronts are identified with heteroclinic connections between  $A_{n\pi}$ ,  $n = 0, 1$ .

The Maxwell point  $\gamma_M$  is also the termination point of a pair of branches of small amplitude “standard” oscillons. To locate these we look for small amplitude solutions that

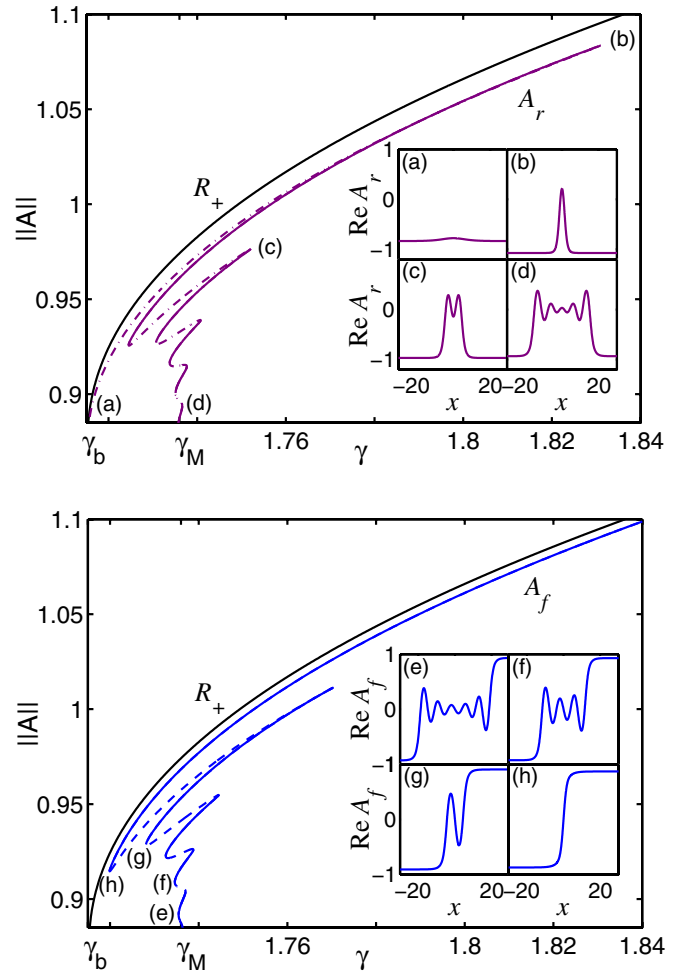


FIG. 2 (color online). Bifurcation diagram for Eq. (2) near the resonance boundary  $\gamma_b$  showing the norm (4) as a function of  $\gamma$  for intertwined branches of reciprocal oscillons ( $A_r$ ) and nonmonotonic fronts ( $A_f$ ) near  $\gamma = \gamma_M$ ; solid lines mark stable solutions. The insets (a), (b), (c), (d) and (e), (f), (g), (h) show the profiles of  $\text{Re}A_r$  and  $\text{Re}A_f$  at the locations indicated in the bifurcation diagrams. The front in (h) is monotonic and so corresponds to an Ising front. The profiles along the stable portions of each branch agree with the results of direct numerical integration of Eq. (2). Parameters:  $\mu = -0.5$ ,  $\nu = 2.0$ ,  $\alpha = 1$ ,  $\beta = 1.1$ ,  $L = 200$ .

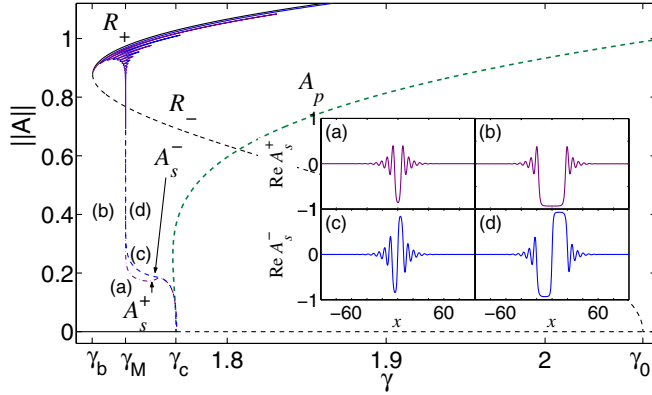


FIG. 3 (color online). Bifurcation diagram for Eq. (2) showing the norm (4) as a function of  $\gamma$  for spatially uniform states ( $|A| = R_{\pm}$ ), spatially periodic states ( $|A| = |A_p|$ ), and spatially localized states of odd ( $|A| = |A_s^-|$ ) and even ( $|A| = |A_s^+|$ ) parity. Solid lines represent stable states. The insets show (a), (b) even parity and (c), (d) odd parity standard oscillons at two different locations,  $\gamma = 1.74$  and  $\gamma = \gamma_M \approx 1.736$ , respectively. Other parameters are as in Fig. 2.

bifurcate from the uniform trivial state  $A = 0$ . Equation (2), linearized about  $A = 0$ , has solutions of the form  $A \propto \exp(\lambda x)$ . At  $\gamma = \gamma_c \equiv |\nu - \mu\alpha|/\rho$ ,  $\rho \equiv \sqrt{1 + \alpha^2}$ , a pair of pure imaginary eigenvalues  $\lambda = \pm ik_0$ ,  $k_0 = \sqrt{\mu + \nu\alpha}/\rho$ , of double multiplicity is present, corresponding to a reversible Hopf bifurcation in space [14]. When  $\mu + \nu\alpha > 0$ ,  $\alpha < \beta$ , and  $(\alpha + \beta) \times (\mu^2 - \nu^2) - 2\mu\nu(1 - \alpha\beta) < 0$  (so that  $\gamma_c > \gamma_b$ ) weakly nonlinear analysis in the vicinity of  $\gamma_c$  reveals the simultaneous presence of small amplitude spatially periodic solutions

$$A_p(x) = \sqrt{2q}(\eta + i) \cos(k_0 x + \varphi), \quad (5a)$$

and small amplitude spatially localized solutions given by

$$A_s(x) = 2\sqrt{q}(\eta + i) \text{sech}(\sqrt{p}x) \cos(k_0 x + \varphi). \quad (5b)$$

The latter correspond to the standard oscillons since they asymptote to  $|A| = 0$  as  $x \rightarrow \pm\infty$ . Since  $q = (\gamma_c - \gamma)/3\eta(\beta - \alpha)$ ,  $\eta = \alpha + \rho$ , and  $p = \gamma_c(\gamma_c - \gamma)/2\rho^2 k_0^2$ , both  $A_p$  and  $A_s$  bifurcate subcritically. Terms beyond all order select solutions with  $\varphi = 0, \pi/2, \pi, 3\pi/2$  [15]. Consequently, we distinguish in (5b) between families of even ( $A_s^+$ ;  $\varphi = 0, \pi$ ) and odd ( $A_s^-$ ;  $\varphi = \pi/2, 3\pi/2$ ) parity standard oscillons, satisfying  $A_s^{\pm}(-x) = \pm A_s^{\pm}(x)$ . On an infinite domain ( $L = \infty$ ) the  $A_s^{\pm}$  branches terminate monotonically, as  $\gamma$  decreases, at the Maxwell point  $\gamma = \gamma_M$ , where the  $A_s^+$  states form a pair of stationary fronts connecting the  $A = 0$  state and either  $A_0 = R_+ \exp(i\phi_0)$  or  $A_{\pi} = R_+ \exp(i\phi_{\pi})$ , while the  $A_s^-$  states form three fronts connecting  $A = 0$ , and both  $A_0$  and  $A_{\pi}$ ; cf. Figure 3. Stability computations reveal that in the absence of additional interactions the standard oscillons of either parity are unstable in  $\gamma_M < \gamma < \gamma_c$  (Fig. 3).

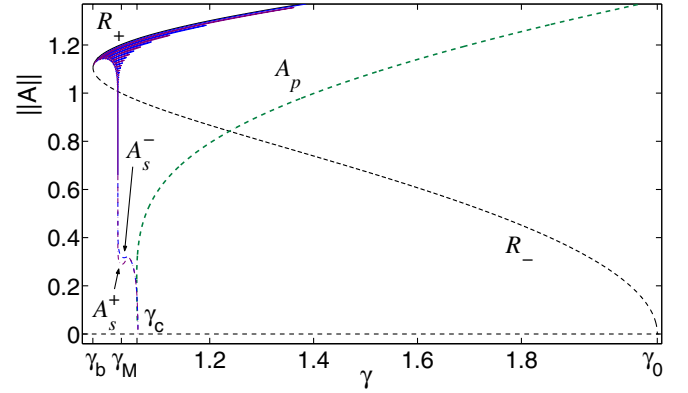


FIG. 4 (color online). Corresponding bifurcation diagram for  $\mu = 0.5$ . Other parameters are as in Fig. 2.

On an infinite domain the four families  $A_s^{\pm}$ ,  $A_r$ ,  $A_f$  of localized solutions remain distinct, and all four terminate at  $\gamma_M$ ; on a finite domain, however, they reconnect pairwise near  $\gamma_M$  with the small amplitude localized states  $A_s^+$  connecting to the large-amplitude reciprocal oscillons  $A_r$ , and  $A_s^-$  connecting to  $A_f$ . Thus the  $A_s^+$  branch terminates at the saddle node at  $\gamma_b$  while the  $A_s^-$  branch extends to large  $\gamma$ ; cf. [16]. This metamorphosis can only occur via the heteroclinic states present at  $\gamma_M$  because only these states contain “infinite” portions of both  $A = 0$  and  $A = A_{n\pi}$  states.

Analysis of the self-exciting oscillatory case,  $\mu > 0$ , reveals a similar bifurcation structure (Fig. 4). The main difference resides in the stability of the trivial state  $A = 0$  which is now unstable to spatially uniform perturbations. As a result the stability properties of both the reciprocal oscillons and the fronts start to differ once these begin to interact with  $A = 0$  near  $\gamma = \gamma_M$ . This can lead to the formation of localized but nonresonant states and will be discussed elsewhere.

Direct numerical integration of the two-dimensional FCGL Eq. (2) supports the results obtained from the above analysis in one dimension. Figure 1 shows the resulting stable axisymmetric reciprocal oscillons, while Fig. 5 shows the corresponding results for the frontlike solutions (right insets) and phase kinks [17] (left insets). All of these two-dimensional solutions exist within the region of stability of the one-dimensional reciprocal oscillons  $A_r$  (shaded dark) and nonmonotonic fronts  $A_f$  (shaded light), obtained by tracking the location of the saddle nodes at which these states lose stability in one dimension. In all cases we used a generic initial condition consisting of a small random perturbation around the trivial state  $A = 0$  embedded in a background of phase-locked states. Because of curvature effects the thresholds for these two-dimensional states need not coincide with the thresholds computed in one dimension. Nevertheless, the one-dimensional analysis appears to delimit the existence region of stable two-dimensional localized states.

In this Letter we have discussed the mechanisms that lead to the presence of a large albeit finite multiplicity of

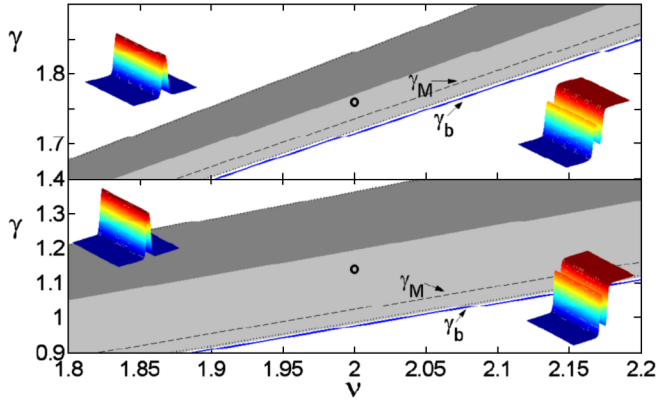


FIG. 5 (color online). Profiles of a stable nonmonotonic front  $\text{Re}A_f$  (right) and a stable phase kink  $\text{Re}A_r$  (left), obtained (open circles) via two-dimensional numerical integration of Eq. (2) on  $x = [0, 50]$ ,  $y = [0, 200]$  with Neumann boundary conditions ( $y$  along the front) for parameter values similar to those for the axisymmetric states in Figs. 1(a) and 1(b). The upper panel corresponds to the damped oscillatory regime with dark shading indicating the region between outermost saddle-node bifurcations bounding stable reciprocal oscillons  $A_r$ , and light shading indicating the corresponding stability region for the nonmonotonic fronts  $A_f$ , as computed from one-dimensional theory. Since the former and the latter domains overlap (see Fig. 2), the dotted line between  $\gamma_M$  and  $\gamma_b$  marks the lower (leftmost) limit of the  $A_r$  region. The lower panel shows the corresponding results for the self-exciting regime.

stable large-amplitude (reciprocal) oscillons, fronts and phase kinks both in damped and self-exciting oscillatory systems. The theory shows that formation of both reciprocal oscillons and Ising fronts should be expected near the boundary of the 2:1 resonance tongue. Moreover, since labyrinthine patterns generally develop through a transverse instability of Ising fronts [6,8], it is natural to expect coexistence between reciprocal oscillons and labyrinthine patterns. Additional support for this suggestion is provided by the fact that the widths of the reciprocal oscillons and the fronts are comparable [see Figs. 2(a) and 2(h)], a conclusion that is consistent with experimental observations [7]. Although a direct link between the FCGL model and the experiments on driven granular or BZ systems remains to be established, we believe that the qualitative behavior described here is independent of the specific models used to describe these systems, provided a region of coexistence between the spatially uniform trivial and nontrivial states is present and contains a Maxwell point. Within gradient systems the presence of such a point is generally simple to establish, and its presence simplifies the relation between localized states in one and two dimensions [18]. In nonvariational systems such as the one studied here this simplification is absent and extensions of the theory to two spatial dimensions remain to be worked out. We expect, however, that the basic scenario described here will also apply to other systems exhibiting bistability such as reaction-diffusion systems.

We thank A. Lin, B. Marts, and J. Fineberg for helpful discussions. This research was supported by NASA under Grant No. NNCO4GA47G and NSF under Grant No. DMS-0305968.

\*Present address: Department of Medicine (Cardiology), University of California, Los Angeles, CA 90095, USA.

- [1] L. Stenflo and M. Y. Yu, *Nature (London)* **384**, 224 (1996).
- [2] P. B. Umbanhowar, F. Melo, and H. L. Swinney, *Nature (London)* **382**, 793 (1996).
- [3] V. Petrov, Q. Ouyang, and H. L. Swinney, *Nature (London)* **388**, 655 (1997).
- [4] S. Longhi, *Opt. Commun.* **149**, 335 (1998); O. Lioubashevski, Y. Hamiel, A. Agnon, Z. Reches, and J. Fineberg, *Phys. Rev. Lett.* **83**, 3190 (1999).
- [5] L. S. Tsimring and I. S. Aranson, *Phys. Rev. Lett.* **79**, 213 (1997); D. H. Rothman, *Phys. Rev. E* **57**, R1239 (1998); C. Crawford and H. Riecke, *Physica (Amsterdam)* **129D**, 83 (1999); A. Yochelis, B. Galanti, and Z. Olami, *Phys. Rev. E* **60**, 6157 (1999); T.-C. Jo and D. Armbruster, *Phys. Rev. E* **68**, 016213 (2003).
- [6] D. Blair *et al.*, *Phys. Rev. E* **61**, 5600 (2000).
- [7] B. Marts, K. Martinez, and A. L. Lin, *Phys. Rev. E* **70**, 056223 (2004).
- [8] A. Yochelis *et al.*, *SIAM J. Appl. Dyn. Syst.* **1**, 236 (2002); A. Yochelis, C. Elphick, A. Hagberg, and E. Meron, *Physica (Amsterdam)* **199D**, 201 (2004).
- [9] J. M. Gambaudo, *J. Diff. Equ.* **57**, 172 (1985); C. Elphick, G. Iooss, and E. Tirapegui, *Phys. Lett. A* **120**, 459 (1987).
- [10] P. Couillet, J. Lega, B. Houchmanzadeh, and J. Lajzerowicz, *Phys. Rev. Lett.* **65**, 1352 (1990).
- [11] The coefficients are given by  $\xi \equiv [\nu(1 - \beta^2) + \varrho\tilde{\mu} - 2\mu\beta]/[\mu(\beta^2 - 1) + \varrho\tilde{\nu} - 2\nu\beta]$ ,  $a \equiv c_2\sqrt{\gamma - \gamma_b}/c_3$ ,  $b \equiv c_2\sqrt{\gamma - \gamma_b}/c_1$  where  $c_1 \equiv U_b[(4\beta - 3\sigma)\xi^2 + 2\beta(\sigma\xi + 2) - \sigma] + V_b(\xi^2 + 2\beta\xi + 3)$ ,  $c_2 \equiv U_b\{\tilde{U}_b[\sigma(3\xi - \beta) - 4\beta\xi] + \tilde{V}_b[\sigma(1 - \beta\xi) - 4\beta]\} - V_b[\tilde{U}_b(\beta + \xi) + \tilde{V}_b(3 + \beta\xi)]$ ,  $c_3 \equiv \sigma(\xi - \alpha) - \xi\alpha - 1$ ,  $\sigma \equiv \beta + \varrho$ ,  $U_b \equiv \sqrt{\sigma/2\varrho R_b}$ ,  $V_b \equiv \sqrt{(\varrho - \beta)/2\varrho R_b}$ ,  $\tilde{U}_b \equiv R_b[\varrho^2\gamma_b - \mu(\beta^2 - 1) + 2\nu\beta]/2\tilde{\mu}\sqrt{\varrho^2\gamma_b + \beta\tilde{\nu}}$ ,  $\tilde{V}_b \equiv R_b[\varrho^2\gamma_b + \mu(\beta^2 - 1) - 2\nu\beta]/2\tilde{\mu}\sqrt{\varrho^2\gamma_b - \beta\tilde{\nu}}$ ,  $R_b \equiv \sqrt{\tilde{\mu}/\varrho}$ .
- [12] E. Doedel *et al.*, “*AUTO2000: Continuation and Bifurcation Software for Ordinary Differential Equations (with HOMCONT)*,” Technical report, Concordia University (2002).
- [13] Y. Pomeau, *Physica (Amsterdam)* **23D**, 3 (1986); J. Burke and E. Knobloch, *Phys. Rev. E* **73**, 056211 (2006).
- [14] G. Iooss and M. C. Pérouème, *J. Diff. Equ.* **102**, 62 (1993).
- [15] G. Kozyreff and S. J. Chapman, *Phys. Rev. Lett.* **97**, 044502 (2006).
- [16] P. D. Woods and A. R. Champneys, *Physica (Amsterdam)* **129D**, 147 (1999); J. Knobloch and T. Wagenknecht, *Physica (Amsterdam)* **206D**, 82 (2005).
- [17] H. Chaté, A. Pikovsky, and O. Rudzick, *Physica (Amsterdam)* **131D**, 17 (1999).
- [18] A. Hagberg *et al.*, *Physica (Amsterdam)* **217D**, 186 (2006).